RESEARCH ARTICLE

Rapid improvement in thermostability of GH11 xylanase (XynASP) from *Aspergillus saccharolyticus* JOP 1030-1 by tryptophan residue substitution

Tongbiao Li, Xiaoli Zhu, Mingyang Ye, Mingcheng Wang, Jinjin Zhu, Fujia Shen, Enzhong Li*

School of Biological Science and Food Engineering, Huanghuai University, Zhumadian, Henan 463000, China

Received: January 15, 2022; **accepted:** February 11, 2021.

Poor thermal stability is the main limiting factor for the industrial application of xylanase. To explore the way to improve the thermal stability of xylanase and obtain thermostable xylanase, a mesophilic xylanase gene (*xynASP*) (GenBank accession number: XM_025579666.1) derived from *Aspergillus saccharolyticus* JOP 1030-1 was mined by using the BLAST program and *Thermomonospora fusca* xylanase gene (*TfxA*) (GenBank accession number: KF927166.1) as the probe. The mined gene without signal peptide was cloned into *Escherichia coli* BL21 (DE3) cells by using the pET-28a expression system. Enzymatic characterization and conformation analysis showed that the recombinant XynASP belonged to GH11 family mesophilic xylanase with poor heat resistance, which limits the industrial applications of the enzyme at high temperature conditions. To rapidly enhance thermostability, the aromatic amino acids tryptophan was introduced at the 41st site of N-terminal of recombinant XynASP to design the variant T41W. The results experimentally confirmed that the beneficial variant T41W displayed the optimum temperature increased by 10°C comparing to that of the wild type XynASP. The half-life of inactivation of the variant T41W increased to 127.7 min at 45°C, which was approximately 6.2-fold longer than that of the wild type and exhibited a substantially improved thermostability. In addition, the variant T41W exhibited a high stability after incubated with metal ions and different concentrations of various organic solvents (methanol, ethanol, and isopropanol), which was similar to that of the wild type XynASP. This study demonstrated that the enzyme could be rapidly designed and substantially improved thermostability by site-directed mutagenesis. The resulted variant T41W could be a prospective candidate for industrial application.

Keywords: xylanase; thermostability; site-directed mutagenesis; xylan.

***Corresponding author:** Enzhong Li, School of Biological Science and Food Engineering, Huanghuai University, Zhumadian, Henan 463000, China. Phone: +86 039 6285 3517. E-mail: lez1219@163.com.

Introduction

Xylan polymerized from xylose and arabinose by β-1,4-glycosidic bond is a primary component of plant hemicelluloses and one of the most abundant biomass energies besides cellulose. Because of the complex chemical structure, xylan becomes difficult to be applied directly or even harmful in many industries [1]. Xylanases (EC 3.2.1.8) randomly hydrolyze the β-1,4-glycosidic bond of xylan to produce reducing xylo-oligosaccharides with different lengths, which are considered to be the key enzyme for the degradation of xylan [2]. Xylanases have a wide range of sources, and some organisms have been reported to produce xylanases such as marine algae, bacteria, fungi, yeast, crustaceans, terrestrial plants, and invertebrates, *etc*. [3].

However, xylanases used in biological research are mainly derived from microorganisms [4].

Based on catalytic domain sequence similarity, xylanases are classified into glycoside hydrolase (GH) families 5, 7, 8, 10, 11, 26, 30, and 43 [5]. In recent decades, lots of research had mainly focused on only two of the xylanases, GH10 and GH11 families, which had exhibited the great potential for industrial application. The structure of GH10 xylanase is mainly composed of eight pairs of (β/α) folded casks, which are complex and multi-domain enzymes including cellulose-binding domain, thermostable domain, catalytic domain, and linking sequences. GH11 xylanases are composed of two twisted antiparallel β-sheets and one single α-helix that forms the structure resembling the shape of a partially closed right hand, which employ the double exchange catalytic mechanism using two glutamates (Glu) as the catalytic residues [6-8]. Because of the simple structure of GH11 xylanases, excellent substrate specificity, and high catalytic activity, GH11 xylanases have become crucial industrial enzyme preparations and more suited for industrial applications including chemical engineering, feed manufacture, pulp bleaching, food processing, and next generation bio-refinerie [9-11]. Meanwhile, improved characteristics of GH11 family xylanases towards heat resistance, catalytic activity, and pH stability had been extensively studied [12-14]. Among them, the improvement of thermostability for GH11 xylanases has become a crucial study area owing to the heat-resistance requirement in various industrial conditions and poor thermal stability of natural GH11 xylanases, which also has become the bottleneck of their industrial application [15-16]. Several studies have been carried out to enhance the thermostability of xylanases with protein engineering, which contained different strategies such as directed evolution approaches and rational/semi-rational design [10, 17-19]. Numerous studies showed that site-directed mutagenesis was an available and effective design approach of the thermostable variants while avoiding laborious high-throughput [20-23]. A growing number of xylanases have been engineered to improve heat resistance *via* the construction of hydrogen bonds, salt bridges, hydrophobic and disulfide bonds [9, 24-26]. Meanwhile, the interaction of aromatic groups of aromatic amino acids at the N-terminal plays an important role in maintaining the stability of conformation and improving the thermal stability of GH11 xylanase that has been confirmed by Georis, *et al*. [27].

To speed up the industrial application, many xylanases' genes have been isolated from nature with traditional biological methods [24]. In the post-genome era, the rapid increase of biological information has brought unprecedented opportunities for the discovery and development of biocatalysts. With the development of bioinformatics and the rapid accumulation of new genomic information, the functional mining technology of genetic data has been rapidly developed. In recent years, many highly efficient enzymes have been mined by using genomic data mining technology [28]. This study applied genomic data mining technology and gene cloning and expression method to explore the way to improve the thermal stability of xylanase and obtain thermostable xylanase.

Materials and methods

The mining and construction of the recombinant xylanase

By using *Thermomonospora fusca* GH11 family xylanase gene *TfxA* (GenBank accession number: KF927166.1) as the probe, the gene *xynASP* (GenBank accession number: XM_025579666.1) was analyzed and obtained by sequence alignment using the BLAST program (https://blast.ncbi.nlm.nih.gov/Blast.cgi). The signal peptide of *xynASP* was determined and eliminated by using SignalP 5.0 server (http://www.cbs.dtu.dk/services/SignalP/) and DNAMAN program (https://www.lynnon.com/desktop.html). To construct the recombinant plasmid pET-28a-xynASP, the whole *xynASP* gene synthesized at Sangon Biotech (Shanghai, China)

without signal peptide was inserted into multiple cloning sites (*EcoR* I and *Hind* III) of the pET-28a vector (Novagen, Madison, WI, USA), and then, was transformed into *E. coli* BL21 (DE3) (Novagen, Madison, WI, USA).

Homology modeling and prediction of thermostability

The amino acid sequence of XynASP without signal peptide was submitted to the I-TASSER server (https://zhanglab.dcmb.med.umich.edu/I-TASSER/) for homology modeling [31]. The most reliable model, basis on the C-score, was selected and further optimized and evaluated with Discovery Studio 3.0 (https://discover.3ds.com/discovery-studio-visualizer-download). Sequence analysis was performed by using the BLAST program. XynASP functional sites were predicted by using PROSITE (https://prosite.expasy.org/). Physiochemical properties of the recombinant xylanase were identified by using ProtParam (https://web.expasy.org/protparam/). The thermal stability mechanism of the variant toward intramolecular interactions was explained by using the DynaMut (http://biosig.unimelb.edu.au/dynamut/) [32] with the default parameters. The structure of xylanases were visualized and analyzed with PyMOL (https://pymol.org/2/) and Discovery studio 3.0.

Site-directed mutagenesis

The mutant XynT41W was constructed by substituting Thr (T) with Trp (W) at 41st position. Using pET-28a-XynASP as the template, the mutated plasmid pET-28a-XynT41W was rapidly constructed with Quikchange Mutagenesis protocol [33]. Briefly, the PCR procedures were as follows: 98°C for 3 min followed by 25 cycles of 98°C for 30s, 55°C for 45s, 72°C for 2 min; and then, 72°C for 10 min. PCR amplification of T41W mutation was performed by using forward primer T41W-F (5´-TAC TAC TCC TTC TGG TGG GAT GGT GCA AGC GGA-3´) and reverse primer T41W-R (5´-TCC GCT TGC ACC ATC CCA CCA GAA GGA GTA GTA-3´), which were synthesized at Sangon Biotech (Shanghai, China). In the forward and reverse primers, the underlined sequences represent the mutation sites. After digestion with *Dpn* I (New England Biolabs, Beverly, MA, USA) for 1 h at 37°C, the PCR products were transformed into *E. coli* DH5α cells (Novagen, Madison, WI, USA) by heat-shock transformation method, and then, plated to Luria-Bertani (LB) (0.5% yeast extract, 1% peptone, and 1% NaCl) agar plates supplemented with 50 µg/mL of Kanamycin for screening the positive clones. The successful introduction of the variant was confirmed by sequencing at Sangon Biotech (Shanghai, China).

Protein expressions and purification

pET-28a-XynT41W and pET-28a-XynASP were transformed into *E. coli* BL21 (DE3) for protein expression, respectively. A single colony was cultivated in 2 mL of LB medium containing Kanamycin (50 µg/mL) at 37°C overnight. Then, the bacterial suspension (1 mL) was inoculated into 100 mL of Terrific Broth (TB) medium (1.2% peptone, 2.4% yeast extract, 0.4% glycerin, 17 mM KH_2PO_4, and 72 mM K_2HPO_4) for cultivation at 37°C with shaking at 180 rpm. After shaking flask culture for 3 h (the concentration of recombinant *E. coli* cells reached OD_{600} 0.5-0.6), the expression was induced by the addition of 2 mM of isopropyl β-D-1-thiogalactopyranoside (IPTG) and continuation of incubation at 30°C for 2 h. Cells were collected by centrifugation at 6,000 rpm for 10 min at 4°C. The cells were re-suspended with 10 mL of Na_2HPO_4-citric acid buffer (pH 4.6), and then, treated with ultrasonic for cell wall-breaking. To obtain the supernatant containing the enzyme, the cell debris was removed by centrifugation at 10,000 rpm for 20 min at 4°C. The enzyme was purified by Ni-NTA Sefinose™ Resin Kit (Sangon Biotech, Shanghai, China). The purification was carried out following manufacturer's instructions. The homogeneity of the purified enzyme was analyzed by sodium dodecyl sulphate-polyacrylamide gel electrophoresis (SDS-PAGE). Coomassie brilliant blue (R-250) methods were used to determine protein concentration with bovine serum albumin (BSA) as the standard.

Enzyme activity assays

According to the 3,5-dinitrosalicylic acid (DNS)

method, the activity of xylanase was analyzed by measuring the release of reducing sugar from beechwood xylan. The standard assay for xylanase activity was performed at 40°C for 15 min in Na_2HPO_4-citric acid buffer (pH 4.6). The reaction mixture (2.5 mL) contained 1.5 mL of the diluted enzyme solution and 1.0 mL of 0.5% beechwood xylan (Sigma Aldrich Chemicals, St. Louis, Missouri, USA). The reaction was stopped by the addition of 2.5 mL of DNS reagent. The product was quantified at OD_{540} against the substrate blank. Under the above conditions, one unit (U) was defined as the amount of enzyme consumed to produce 1 µmol of reducing sugar per minute as the standard.

Measurements of temperature and pH characteristics for the recombinant xylanases

The purified xylanase was subjected to enzymatic characterization by using the DNS methods. To determine the optimum temperature, the purified enzymes were incubated at different temperatures of 35°C, 40°C, 45°C, 50°C, 55°C, and 60°C with 0.5% beechwood xylan in Na_2HPO_4-citric acid buffer (pH 4.6). To measure the thermostability of the purified xylanase, the enzyme without containing substrate were pre-incubated for 2 h at 45°C and 50°C, respectively. Samples were taken to the ice after every 10 min and residual activities of samples were determined under standard assay conditions. The control activity was estimated without pre-incubation of the enzyme.

The optimal pH of the enzymes was determined at the optimal temperature by incubation in different pH (3.0 - 8.0) buffers. After optimization of the recombinant xylanase assay, the enzyme was subjected to a stability test using different parameters. All assays in this work were performed in triplicate. The pH stability with variable pH buffer (4.0, 5.0, and 6.0) was determined for the wild type and variant T41W by the pre-incubated of the enzyme for 1 h in 200 mM buffer. Corresponding to different pH, the residual activity of the purified xylanase was performed with reference to the standard assay conditions. The various pH buffers were confected as follows: Na_2HPO_4-citric acid buffer (pH 4.0 and 5.0) and Na_2HPO_4-NaH_2PO_4 buffer (pH 6.0). The control without subjecting to pre-incubation was placed on ice. All experiments were carried out in triplicate.

Effect of metal ions and organic solvents

The effects of various metal ions (Ca^{2+}, Mg^{2+}, Na^{+}, Fe^{2+}, K^{+}, Cu^{2+}, Fe^{3+}, Zn^{2+}, and Mn^{2+}) were analyzed by pre-incubating enzymes in 1 mM of metal ion solution for 1 h at 25°C. The residual activity was analyzed and compared to the control. The control was determined in parallel without pre-incubating metal ions. To demonstrate the tolerance of xylanase to organic solvents, enzyme was pre-incubated at various concentrations (10 %-30 %) of different solvents (ethanol, methanol, isopropanol), and then, residual activities of all the samples were estimated under standard assay conditions. All experiments were carried out in triplicate.

Results and discussion

Gene mining and construction of the recombinant XynASP

The mined xylanase gene (702 bp) derived from *Aspergillus saccharolyticus* JOP 1030-1 and encoding 234 amino acids was screened by using the gene *TfxA* [34] as the probe for gene mining. In the gene mining of enzymes, amino acid sequence similarity between 30% and 70% was generally considered to retain some functions similar to the probe enzyme while having certain specificity. The amino acid sequence of screened xylanase was identified with 60.87% similarity to the probe TfxA by the BLAST program, which was inferred that new specificity of screened xylanase could be identified comparing to that of TfxA. The signal peptide sequence of screened xylanase was predicted to contain 19 amino acid residues by signalP 5.0 and was removed by the DNAMAN program. The screened xylanase gene without signal peptide, named *xynASP*, consisted of 645 bp and encoded 215 amino acids, which was used to construct the recombinant expression plasmid with pET-28a vector by whole-gene synthesis.

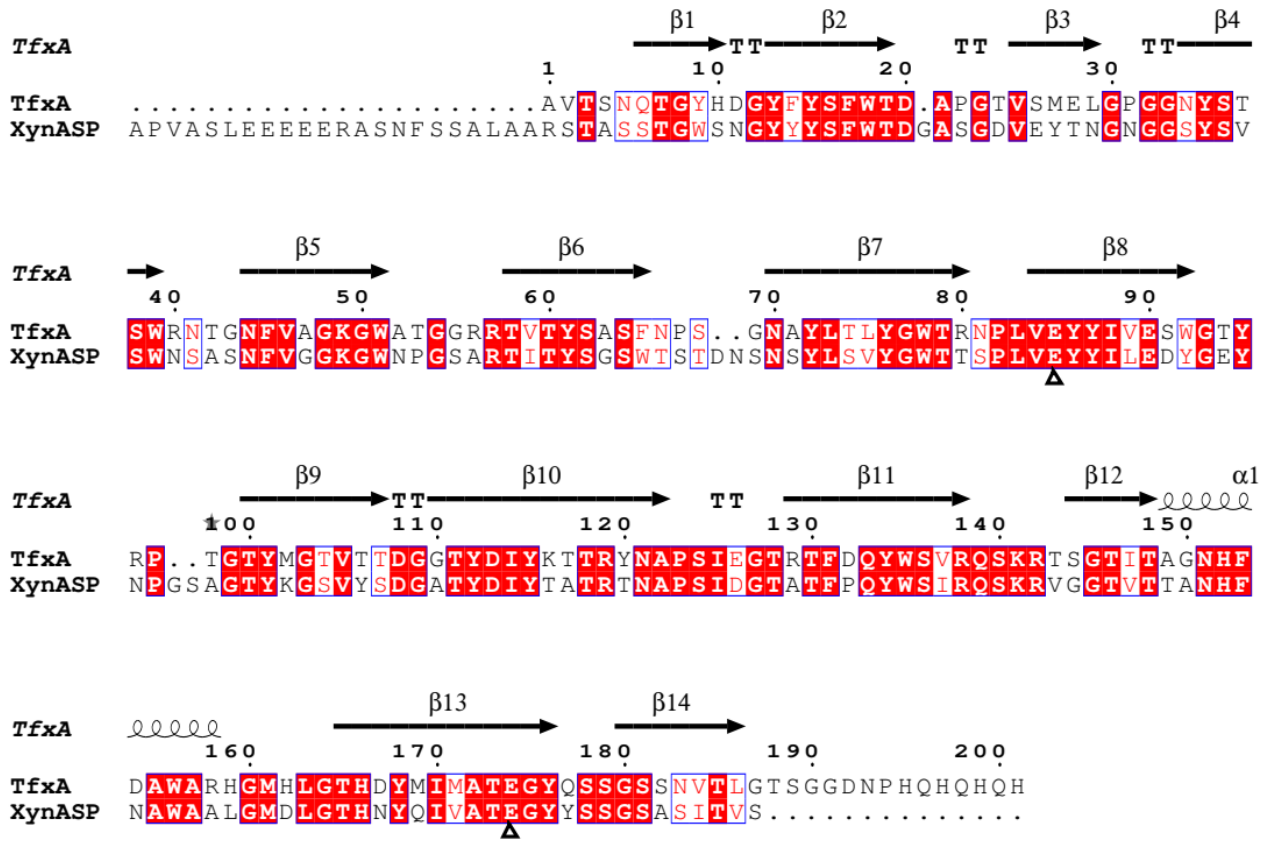

Figure 1. Sequence alignment of XynASP. Amino acids highlighted in light red color represent fully conserved region. Catalytic residue (Glu-Glu) was shown in black triangle.

Then, pET-28a-XynASP was transformed into *E. coli* BL21 for amplification of recombinant strains.

Sequence analysis of the recombinant XynASP

Sequence and secondary structure alignments of XynASP and TfxA (PDB 3ZSE_A) were performed by using the ESPript 3.0 (https://espript.ibcp.fr/ESPript/ESPript/index.php) (Figure 1) [35]. Although XynASP was different from TfxA in the primary sequence, the secondary structure of XynASP was quite conservative, containing fourteen β-sheets, one α-helix, and conservative catalytic residue (Glu-Glu), which belonged to the GH11 xylanase.

The composition of amino acids in XynASP and TfxA were showed in Table 1. In the amino acid sequence of XynASP, there was higher abundance of serine (15.9%), glycine (11.7%), threonine (10.7%), alanine (9.8%), and tyrosine (9.3%). Methionine (0.5%) and histidine (0.9%) were the lowest compositions, while there was no cysteine residue that prevented the formation of disulfide bonds. In addition, the proportion of arginine, proline, and Thr/Ser in TfxA was found higher than that of XnyASP, which were 1.78, 1.25, and 2.38-fold to that of XnyASP, respectively. The composition and proportion of arginine, proline, and Thr/Ser in thermostable xylanases are significantly higher than that of mesophilic xylanases, acting as the beneficial amino acid residues for the stability of protein structure, and playing a crucial role in heat resistance. Arginine can form the hydration layer by dipole-charge interaction with medium water, then increasing the stability of protein, which has been confirmed by Sriprang, *et al*. [36]. The interaction of the pyrrole ring of proline with the former residues can enhance the rigidity and

hydrophobicity of protein, resulting in the lower conformation entropy of proline than other amino acids, while the β-sheets linked by proline are more stable [37]. In addition, a higher proportion of Thr/Ser in thermostable xylanases has been reported by Hakulinen, *et al*. [38]. These studies provide a strategy that increases the content of beneficial amino acid residues may improve the heat resistance of XynASP.

Table 1. Composition of amino acid sequences.

Amino acids	Compassion (%)	
	XynASP	TfxA
Ala (A)	9.8	5.5
Arg (R)	2.8	5.0
Asn (N)	6.5	5.5
Asp (D)	3.7	4.0
Cys (C)	0.0	0.0
Gln (Q)	1.4	3.5
Glu (E)	4.7	2.5
Gly (G)	11.7	13.9
His (H)	0.9	4.5
Ile (I)	3.3	2.5
Leu (L)	3.3	3.0
Lys (K)	1.4	1.5
Met (M)	0.5	2.5
Phe (F)	2.3	3.0
Pro (P)	2.8	3.5
Ser (S)	15.9	9.0
Thr (T)	10.7	14.4
Trp (W)	3.7	3.5
Tyr (Y)	9.3	8.5
Val (V)	5.1	4.5

Homology modeling for XynASP and the design of variant T41W

The initial structure of XynASP was successfully constructed by the I-TASSER web server. To remove redundant conformations and supplement non-complete amino acid residues, the initial model was optimized by the Discovery Studio 3.0. Catalytic domain of XynASP resembles a typical β-jelly-roll fold structure, and the catalytic residues E110 and E201 are located at the side of the catalytic active pocket cleft (Figure 2). As assessed by Ramachandran Plot [22], 95% of the dihedral angles of amino acid residues in the model are located at the optimal conformation, and 90% of the residues are inside the allowed region of the plot (Figure 3a). Profile-3D evaluation exhibited that the amino acid compatibility score (verify score) in the model was all above the "0 line", which indicated that the model had a high matching degree with its amino acid sequence (Figure 3b). Based on the above analysis, the optimized model is credible, and the conformation of amino acids are reasonable, which could be used as the ideal structure of XynASP for the design of thermostability.

Based on the sequence analysis of the recombinant XynASP, β2-sheet at the N-terminal was composed of seven amino acid residues (35YYYSFWT41) including 5 aromatic amino acids residues (Figure 1). The high content of aromatic amino acids was beneficial to improve the stability of the protein [28]. To further improve the stability of β2-sheet of XynASP, the threonine (T) at the position of 41 was randomly substituted by tryptophan (W) to construct the potential beneficial variant T41W.

Expression and purification of the wild type XynASP and variant T41W

The wild type XynASP and variant T41W were successfully expressed by using IPTG as an inducer in *E. coli* BL21 cells. The recombinant xylanases were analyzed by sodium dodecyl sulphate polyacrylamide gel electrophoresis (SDS-PAGE) after protein purification (Figure 4). Only one band of approximately 27 kD was shown for the purified wild type XynASP and variant T41W on SDS-PAGE, which was slightly higher than the theoretically predicted value of 23 kDa, and the 36 extra amino acids at the N-terminal fusion peptide (His-Tag) could presumably contribute to the increasing molecular weight.

Temperature characteristics of the recombinant xylanases

To evaluate the optimum temperature, the activity of purified wild type and variant T41W was measured at temperatures ranging from 35

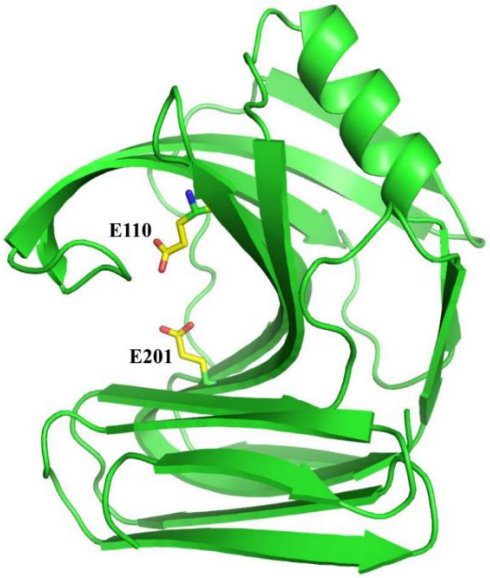

Figure 2. Three-dimensional structure of the wide type XynASP. Yellow sticks represent the catalytic residues E110-E201.

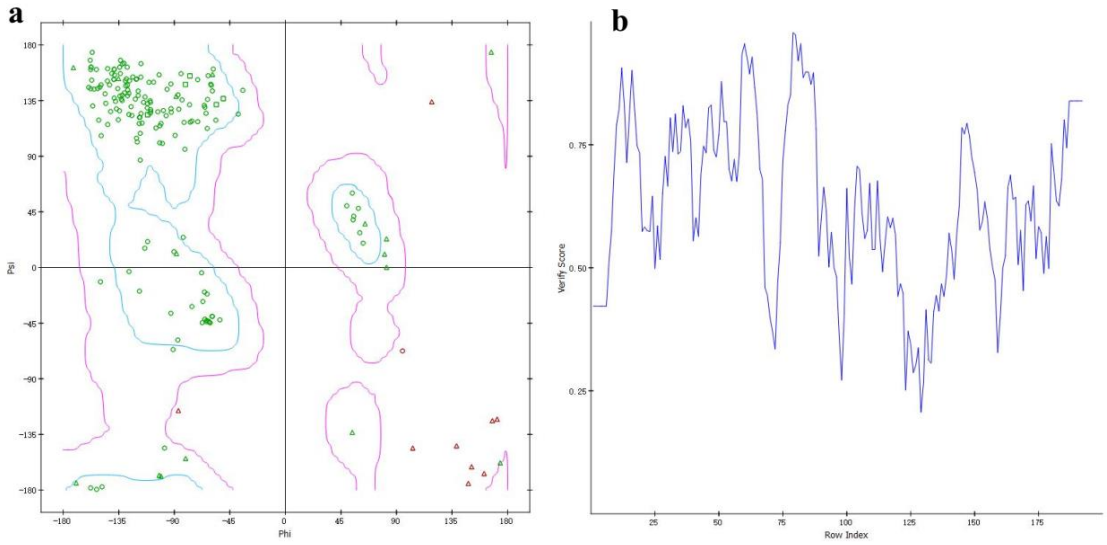

Figure 3. Model evaluation of the wide type XynASP. **(a)** The results of the Ramanchandran Plot evaluation. **(b)** The Profile-3D evaluation.

to 60°C. The optimum temperature of wild type was 45°C, belonging to mesophilic xylanase. However, the optimum temperature of variant T41W was 55°C, which was 10°C higher than that of the wild type. Furthermore, T41W exhibited over 75% relative activity, which was higher than the relative activity (20%) of the wild type at 60°C (Figure 5a). It indicated that the variant T41W acquired a thermophilic property after an extra tryptophan was introduced at 41st position. The wild type and variant T41W were measured for residual activity after incubation in the absence of substrate at 45 and 50°C for 2 h, to identify the thermal stability of the wild type and variant T41W. As shown in Figure 5b, the variant T41W retained 74% of the residual activity after incubation at 45°C for 20 min, whereas the wild type was inactivated rapidly and retained 40% of the original activity with the above incubation conditions. The half-life of thermal inactivation

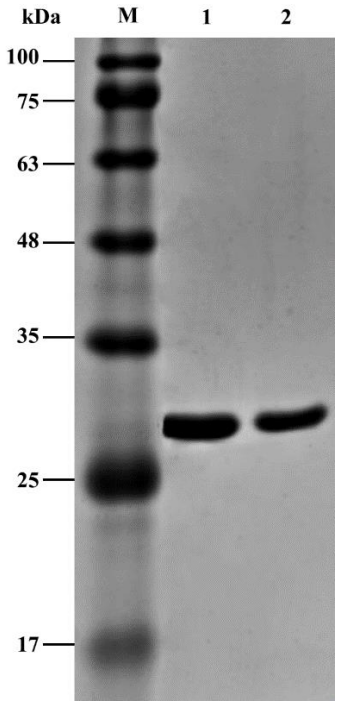

Figure 4. SDS-PAGE analysis of the purified xylanases. **Lane M**: the molecular weight marker. **Lane 1**: the purified XynASP. **Lane2**: the purified T41W.

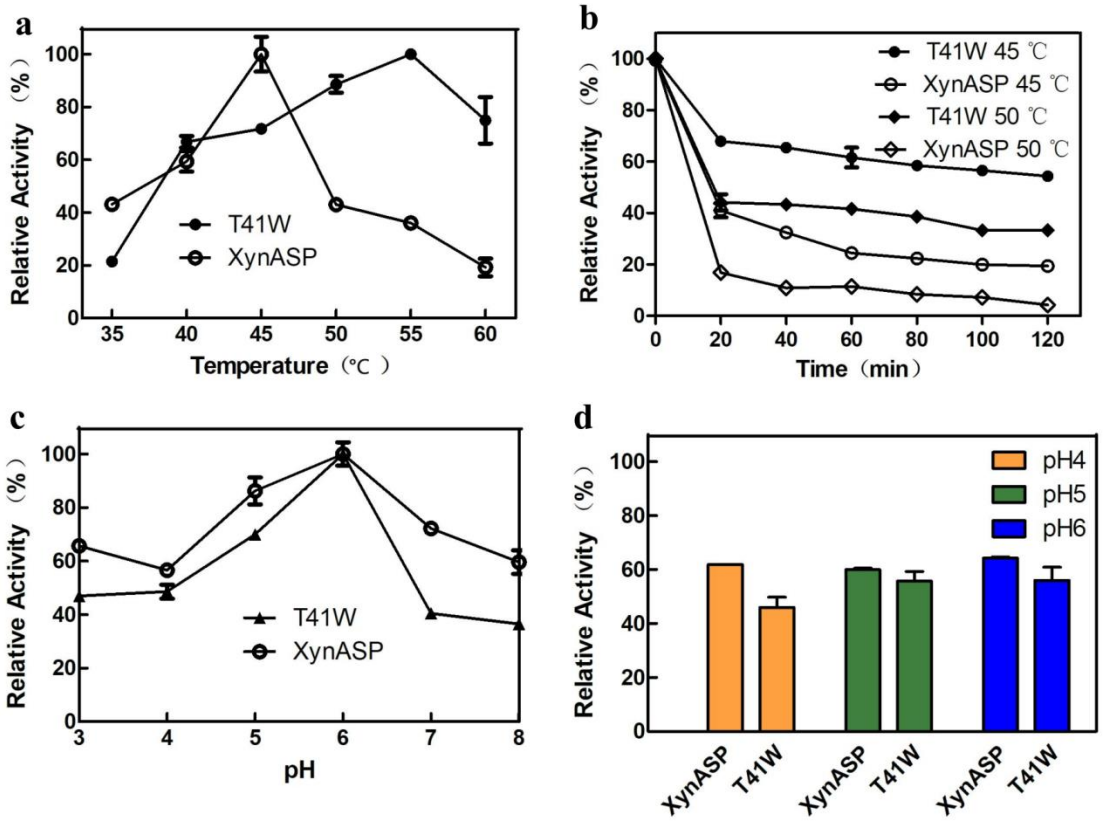

Figure 5. The optimum temperature (a) and thermal stability of the wide type XynASP and variant T41W (b). Optimal pH (c) and pH stability of the recombinant xylanases (d). The mean values of triplicates and the standard deviation (SD) are shown.

was calculated from a linear regression by plotting the natural logarithms of residual activity values versus incubation time. The measured half-life of thermal inactivation of wild type and variant T41W at 45°C ($t_{1/2}$) was 20.7 min and 127.7 min, respectively. This result showed that the half-life of T41W at 45°C was approximately 6.2-fold higher than that of the wild type. After heating treatment at 50°C for 20 min, the residual activity of variant T41W was rapidly lost, with 42% of the residual activities remaining. Subsequently, the residual activity of variant T41W gradually stabilized, and still retained 40% of the activity after heating treatment 2 h. However, the residual activity of wild type decreased rapidly, retaining only 4% of the activity after heating treatment at 50°C for 2 h. Comparing to the wild type, the thermal inactivation pattern of variant T41W demonstrated substantially increased thermal tolerance. These results highlight that the substitution of threonine for tryptophan at 41st position was advantageous for improving the thermal stability of XynASP.

Effect of pH for the recombinant xylanases

The optimal pH of the purified xylanases was investigated with respective optimum temperature at a pH range of 3.0-8.0. The optimal pH of the variant T41W was 6.0, which was similar to that of the wild type (Figure 5c). As shown in Figure 5d, the purified xylanases were incubated between pH 4.0 and 6.0 in the absence of substrate at 40°C for 1 h to determine the pH stability. Comparing to the initial activities, the wild type at pH 4.0-6.0 still had more than 60% residual activity while the pH stability of T41W showed slightly lower than that of the wild type. At pH 4.0, T41W only maintained residual activities of 45.9% while it showed 55.7% and 56.0% at pH 5.0 and 6.0, respectively. In brief, the mutation of threonine to tryptophan at 41st position of the wild type showed similar optimal pH with slightly lower pH stability.

Effect of metal ions and organic solvents for the recombinant xylanases

The effects of metal ions on the activities of the wild type and T41W were significantly different at the same concentration. As shown in Figure 6a, the results illustrated that the activity of the wild type was slightly enhanced after being treated with Mg^{2+}, Na^{+}, and K^{+} at 25°C for 1 h, while Ca^{2+}, Fe^{2+}, Cu^{2+}, and Zn^{2+} were no significant effect on activity of the wild type. The negative effects were found when the addition of Fe^{3+} and Mn^{2+} at 1 mM concentration, which only maintained residual activities of 65.0% and 65.9%, respectively. Fe^{3+} and Mn^{2+} were strongly inhibitor for the wild type, which was inferred that the decline on the activity was due to enzyme precipitation. As known to all, they also could decline the activity of other xylanases [3, 39-40]. The variant T41W altered the effect of certain metal ions on enzymatic activity. When treated with metal ions at the same condition, the variant T41W for Fe^{3+} and Mn^{2+} still maintained residual activities of 99.9% and 71.1%, respectively, which indicated that the tolerance of T41W for Fe^{3+} and Mn^{2+} was significantly higher than that of wild type. However, comparing to the wild type, Mg^{2+} and Na^{+} caused slight decrease in the residual activity of T41W.

Previously, some researchers have reported that xylanases were stable in the presence of organic solvent [41-42]. To analyze the organic solvents tolerance of the variant T41W, the recombinant xylanases were treated with methanol, ethanol, and isopropanol for 1 h at 10%, 20%, and 30% (v/v), respectively. The wild type and variant T41W both still had more than 80% residual activity (Figure 6c and 6d). The data showed that the wild type and variant T41W still retained high residual activities and endured high tolerance for organic solvent. Significantly, the variant T41W retained 95.0% of the residual activity after treated with 30% isopropanol, which was slightly enhanced comparing to that of the wild type (88.6%). For 30% ethanol, the residual activity of wild type was no significant change, while the residual activity of the variant T41W was significantly lower (77.5%) than that of the wild type. These results clarified that substituting

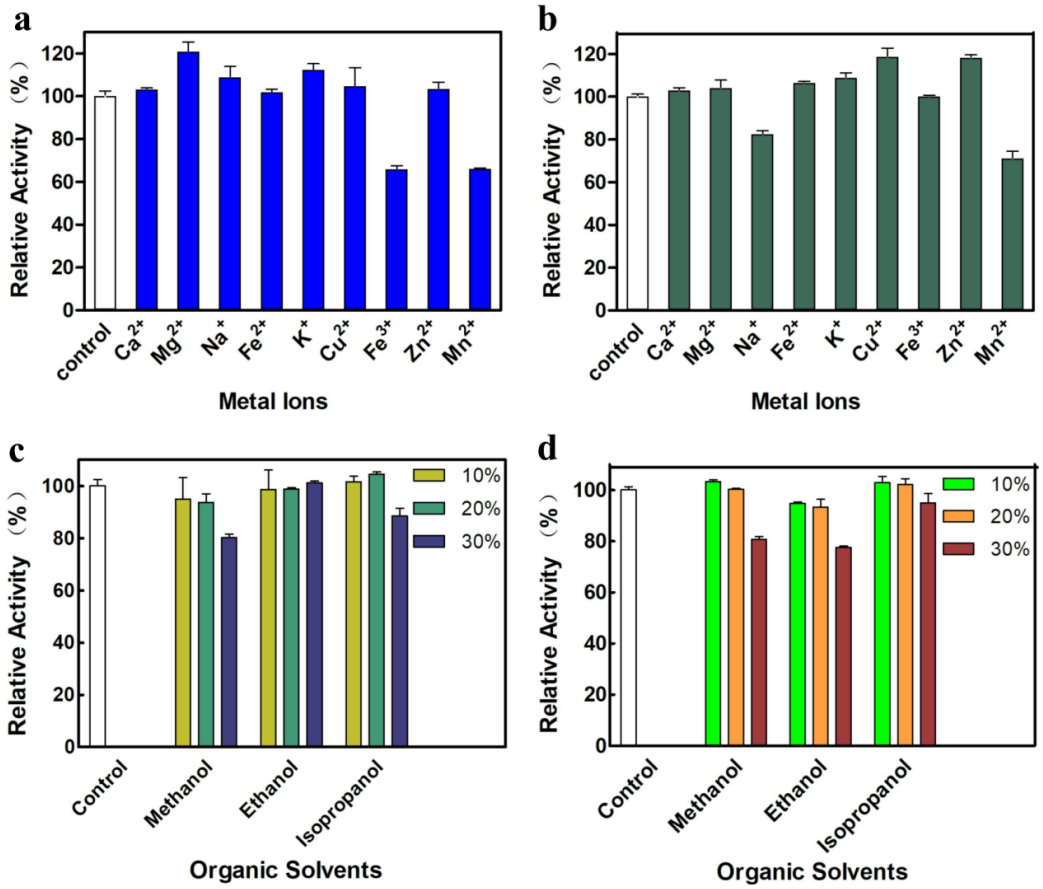

Figure 6. Effect of metal ions and organic solvents on the activity of xylanases. Effects of 1 mM metal ions on the activity of the wide type (a) and the variant T41W (b); effects of organic solvents on the activity of the wide type (c) and the variant T41W (d) at different concentration. The mean values of triplicates and the standard deviation (SD) are shown.

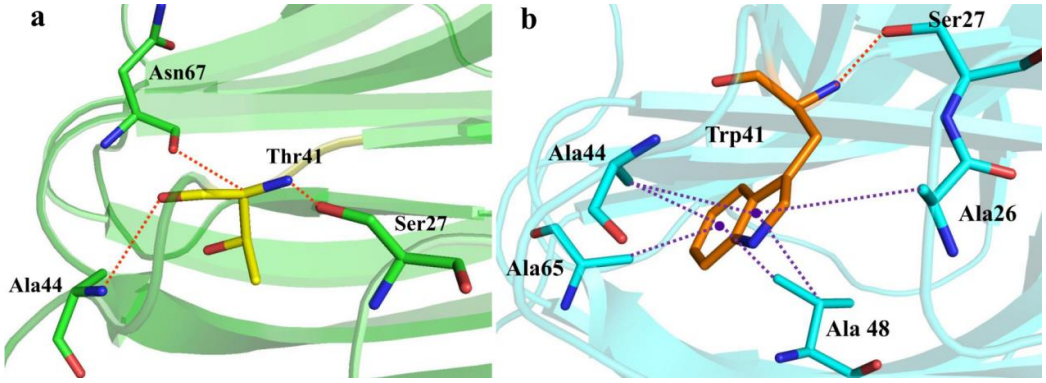

Figure 7. Intramolecular interactions of 41st residue in wild type (a) and variant T41W (b) analyzed by Discovery Studio 3.0. The residues were shown in the stick model. Hydrogen bonds were indicated as red stippled lines, and hydrophobic contacts were shown as purple stippled lines.

threonine (T) at the 41st position with tryptophan (W) on XynASP changed the tolerance to metal ions and organic solvents.

Analysis of possible stabilization mechanisms

Based on the simulated structure of XynASP, Thr41 was located in the flexible loop of the N-

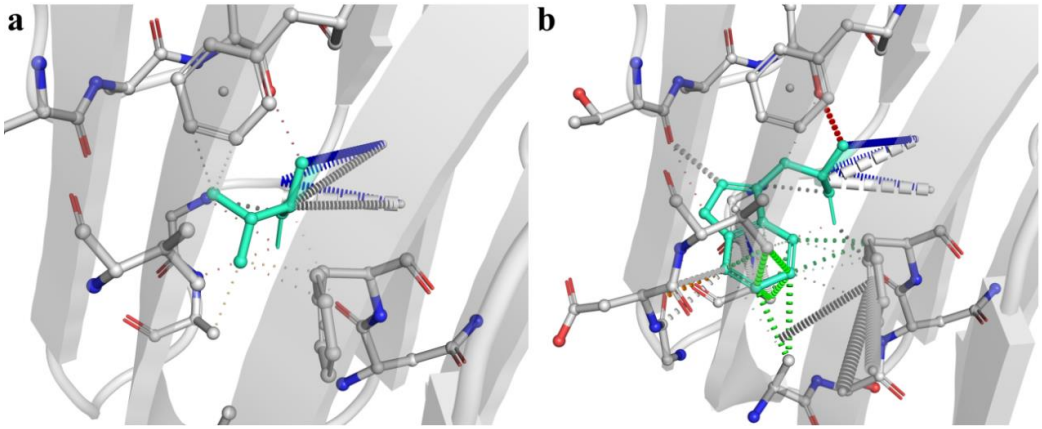

Figure 8. Intramolecular interactions of mutated residue in wild type (a) and variant T41W (b) analyzed by DynaMut. (Notes: cyan stick: the 41st residues; red stippled lines: hydrogen bonds; bule stippled lines: halogen bonds; green stippled lines: hydrophobic contacts.)

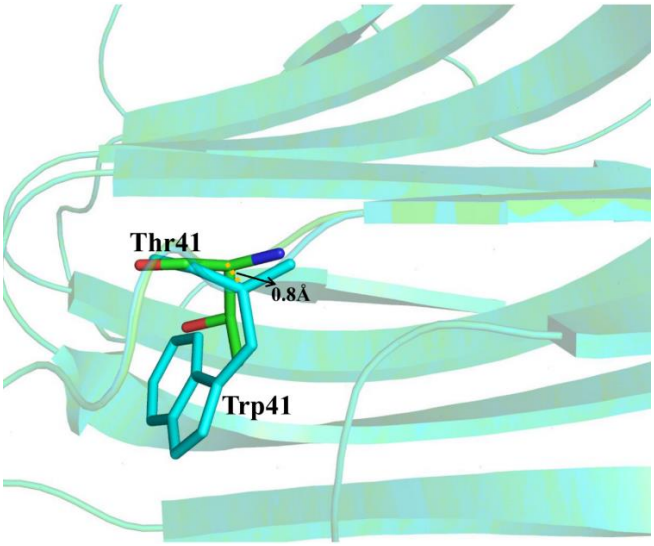

Figure 9. Structure alignment of the wild type and variant T41W.

terminal region (Figure 7a). The structure of T41W was constructed by using XynASP as the template (Figure 7b). Further analysis was focused on the dominant structural factors responsible for protein thermostability such as hydrogen bonds and hydrophobic interactions. The interactions of amino acid residues were predicted by the Discovery Studio 3.0. Hydrogen bonds for the wild type were formed between Trp41 and Ala44, Asn67 (Figure 7a), while the formed hydrogen bonds were broken due to the T41W substitution for the variant T41W (Figure 7b). However, no interaction was found between the 41st amino acid and the surrounding aromatic amino acid residues. Significantly, the T41W substitution formed more hydrophobic interactions with Ala26, Ala44, Ala48, and Ala65 (Figure 7a and 7b), respectively.

The DynaMut server, which can be used to analyze and predict protein stability changes upon the variant, also revealed that the T41W substitution could form more interaction bonds such as halogen bonds and hydrophobic interactions (Figure 8a and 8b) despite the reduction of hydrogen bonds. The added

interaction bonds for T41W could form a more stable and compact N-terminal region. Hydrophobic interactions and hydrogen bonds were predicted by the DynaMut, which were consistent with the results predicted by the Discovery Studio 3.0. The three-dimensional structures of wild type and variant T41W aligned and analyzed by PyMOL clarified that the T41W substitution could cause the Cα of 41st to be shifted 0.8 Å comparing to the wild type (Figure 9). It was inferred that this may be an important factor for the change of interaction bonds. In addition, the vibrational entropy energy ($\Delta\Delta S_{Vib}$ ENCoM: -1.020 kcal/mol.K) and folding free energy (ΔΔGWT-MT: 0.743 kcal/mol) of variant T41W were predicted by the DynaMut server, indicating the decrease of molecule flexibility and the enhancement of protein stability for the variant T41W.

Conclusions

In current work, the mined xylanase gene *xynASP* was expressed in *E. coli* BL21 (DE3) cells by using pET-28a expression system. For the thermal stability design of the XynASP, the high-quality model of enzyme was obtained by the I-TASSER web server. Facilitated by site-directed mutagenesis, the beneficial variant T41W was successfully constructed, which led to a substantially enhanced half-life of thermal inactivation. Heat-resistance mechanisms were explored by computer-aided software and the T41W substitution analysis revealed that W41 gave rise to this enhanced thermal stability. Through the analysis of the intermolecular force of variant T41W, it was found that T41W substitution formed more hydrophobic interactions with the surrounding amino acid residues, which might be the key factor to improve the thermal stability of variant T41W. Meanwhile, similar to the wild type XynASP, the variant T41W still remained the high stability in the presence of organic solvents. The stability of T41W in heat-resistance, metal ions, and organic solvents suggested that the variant T41W may be an attractive candidate in industrial applications.

Acknowledgements

This study was financially supported by the Foundation of Science and Technology Development Project of Henan Province (No. 212102110274, 212102110005, 222102110372); the Foundation of Major Science and Technology Projects of Henan Province (No. 191110110600); the Foundation of Major Science and Technology Projects of Zhumadian City (No. 17702); the Scientific Research Fund of Huanghuai University (No. 12011947); the Key Scientific Research Projects of Colleges and Universities of Henan Province (No. 22A180022); the Scientific and Technological Research Project Foundation of Henan Provincial Scientific and Technological Department (NO. 202102310479); and National scientific research project cultivation fund of Huanghuai University (NO. XKPY-2021003).

References

1. Liu X, Jiang Z, Liu Y, You X, Yang S, Yan Q. 2019. Biochemical characterization of a novel exo-oligoxylanase from *Paenibacillus barengoltzii* suitable for monosaccharification from corncobs. Biotechnol Biofuels. 12:1-14.
2. Juturu V, Wu JC. 2012. Microbial xylanases: Engineering, production and industrial applications. Biotechnol Adv. 30:1219-1227.
3. Chen Z, Liu YL, Zaky AA, Liu L, Chen YY, Li ST, *et al*. 2019. Characterization of a novel xylanase from *Aspergillus flavus* with the unique properties in production of xylooligosaccharides. J Basic Microb. 59:351-358.
4. Abdul B, Junquan L, Kashif R, Jiang W, Lou HQ. 2018. Thermophilic xylanases: from bench to bottle, Crit Rev Biotechnol. 38:1-14.
5. Han NY, Miao HB, Ding JM, Li JJ, Mu YL, Zhou JP, *et al*. 2017. Improving the thermostability of a fungal GH11 xylanase via site-directed mutagenesis guided by sequence and structural analysis. Biotechnol Biofuels. 10:1-12.
6. Li G, Chen X, Zhou X, Huang R, Zhang R. 2019. Improvement of GH10 family xylanase thermostability by introducing of an extra α-helix at the C-terminal. Biochem Bioph Res Co. 515:417-422.
7. Mitra S, Mukhopadhyay BC, Mandal AR, Arukha AP, Chakrabarty K, Das GK, *et al*. 2015. Cloning, overexpression, and characterization of a novel alkali-thermostable xylanase from *Geobacillussp*. WBI. J Basic Microb. 55:527-537.
8. Teng C, Jiang YF, Xu YQ, Li Q, Li XT, Fan GS, *et al.* 2019. Improving the thermostability and catalytic efficiency of GH11 xylanase PjxA by adding disulfide bridges. Int J Biol Macromol. 128:354-362.

9. Bu YF, Cui YL, Peng Y, Hu MR, Tian YE, Tao Y, *et al*. 2018. Engineering improved thermostability of the GH11 xylanase from *Neocallimastix patriciarum* via computational library design. Appl Microbiol Biot. 102:3675-3685.
10. Natesh R, Bhanumoorthy P, Vithayathil PJ, Sekar K , Ramakumar s, Viswamitra MA. 1999. Crystal structure at 1.8 A resolution and proposed aminoacid sequence of a thermostable xylanase from *Thermoascus aurantiacus*. J Mol Biol. 288:999-1012.
11. Collins T, Gerday C, Feller G. 2005. Xylanases, xylanase families and extremophilic xylanases. FEMS Microbiol Rev. 29:3-23.
12. Turunen O, Jnis J, Fenel F, Leisola M. 2004. Engineering the thermotolerance and pH optimum of family 11 xylanases by site-directed mutagenesis. Method Enzymol. 388:156-167.
13. PaëS G, Cortés J, Siméon T, O"Donohue MJ, Tran V. 2012. Thumb-loops up for catalysis: a structure/function investigation of a functional loop movement in a GH11 xylanase. Comput Struct Biotec. 1:1-10.
14. Acevedo JP, Reetz MT, Asenjo JA, Parra LP. 2017. One-step combined focused epPCR and saturation mutagenesis for thermostability evolution of a new cold-active xylanase. Enzyme Microb Tech. 100:60-70.
15. Han N, Ma Y, Mu Y, Tang X, Huang ZX. 2019. Enhancing thermal tolerance of a fungal GH11 xylanase guided by B-factor analysis and multiple sequence alignment. Enzyme Microb Tech. 131:109422.
16. Haki G. 2003. Developments in industrially important thermostable enzymes: a review. Bioresource Technol. 89:17-34.
17. Irfan M, Gonzalez C, Raza S, Rafiq M, Hasan F, Khan S, *et al*. 2018. Improvement in thermostability of xylanase from *Geobacillus thermodenitrificans* C5 by site directed mutagenesis. Enzyme Microb Tech. 111:38-47.
18. Zhang C, Ding Y. 2019. Probing the Relation Between Community Evolution in Dynamic Residue Interaction Networks and Xylanase Thermostability. IEEE ACM T Comput Bi. 99:1-13.
19. Sun Z, Liu Q, Qu G, Feng Y, Reetz MT. 2019. Utility of B-Factors in Protein Science: Interpreting Rigidity, Flexibility, and Internal Motion and Engineering Thermostability. Chem Rev. 119:1626-1665.
20. Muhammed MT, Son Ç, İzgü F. 2019. Three-Dimensional Structure Prediction of Panomycocin, a Novel Exo-β-1,3-Glucanase Isolated from *Wickerhamomyces anomalus* NCYC 434 and the Computational Site-Directed Mutagenesis Studies to Enhance its Thermal Stability for Therapeutic Applications. Comput Biol Chem. 80:270-277.
21. Gao SJ, Wang JQ, Wu MC, Zhang HM, Yin X, Li JF. 2013. Engineering hyperthermostability into a mesophilic family 11 xylanase from *Aspergillus oryzae* by in silico design of N-terminus substitution. Biotechnol Bioeng. 110:1028-1038.
22. Wang J, Tan Z, Wu M, Li J, Wu J. 2014. Improving the thermostability of a mesophilic family 10 xylanase, AuXyn10A, from *Aspergillus usamii* by in silico design. J Ind Microbiol Biot. 41:1217-1225.
23. Li C, Li J, Wang R, Li X, Wu M. 2018. Substituting Both the N-Terminal and "Cord" Regions of a Xylanase from *Aspergillus oryzae* to Improve Its Temperature Characteristics. Appl Biochem Biotech. 185:1044-1059.
24. Beerens K, Mazurenko S, Kunka A, Marques SM, Hansen N, Musil M, *et al*. 2018. Evolutionary Analysis As a Powerful Complement to Energy Calculations for Protein Stabilization. ACS Catal. 8:9420-9428.
25. Yu J, Liu XQ, Guan Ly, Jiang ZQ, Yang SQ. 2020. High–level expression and enzymatic properties of a novel thermostable xylanase with high arabinoxylan degradation ability from Chaetomium sp. suitable for beer mashing - ScienceDirect. Int J Biol Macromol. 168:223-232.
26. Puchart V, Uchová K, Biely P. 2021. Xylanases of glycoside hydrolase family 30 – An overview. Biotechnol Adv. 47:107704.
27. Georis J, de Lemos Esteves F, Lamotte-Brasseur J, Bougnet V, Devreese B, Giannotta F, *et al*. 2000. An additional aromatic interaction improves the thermostability and thermophilicity of a mesophilic family 11 xylanase: structural basis and molecular study. Protein Sci. 9:466-475.
28. Kumar V, Dangi AK, Shukla P. 2018. Engineering Thermostable Microbial Xylanases Toward its Industrial Applications. Mol Biotechnol. 60:226-235.
29. Van Bueren AL, Otani S, Friis EP, Wilson KS, Davies GJ. 2012. Three-dimensional structure of a thermophilic family GH11 xylanase from *Thermobifida fusca*. Acta Crystallogr F. 68:141-144.
30. Wang Q, Xia T. 2008. Enhancement of the activity and alkaline pH stability of *Thermobifida fusca* xylanase A by directed evolution. Biotechnol Lett. 30:937-944.
31. Yang J, Zhang Y. 2015. I-TASSER server: new development for protein structure and function predictions. Nucl Aci Res. 43:174-181.
32. Rodrigues CH, Pires DE, Ascher DB. 2018. DynaMut: predicting the impact of mutations on protein conformation, flexibility and stability, Nucl Aci Res. 46:350-355.
33. Li TB, Zhao FJ, Liu Z, Jin Y, Liu Y, Pei XQ, *et al*. 2019. Structure-guided engineering of ChKRED20 from *Chryseobacterium* sp. CA49 for asymmetric reduction of aryl ketoesters. Enzy Micro Tech. 125:29-36.
34. Sun JY, Liu MQ, Weng XY, Qian LC, Gu SH. 2007. Expression of recombinant *Thermomonospora fusca* xylanase A in *Pichia pastoris* and xylooligosaccharides released from xylans by it. Food Chem. 104:1055-1064.
35. Robert X, Gouet P. 2014. Deciphering key features in protein structures with the new ENDscript server. Nucl Aci Res. 42:320-324.
36. Sriprang R, Asano K, Gobsuk J, Tanapongpipat S, Champreda V, Eurwilaichitr L. 2006. Improvement of thermostability of fungal xylanase by using site-directed mutagenesis. J Biotechnol. 126:454-462.
37. Yang W, Yang Y, Zhang L, Hang X, Guo X, Xu Y, *et al*. 2017. Improved thermostability of an acidic xylanase from *Aspergillus sulphureus* by combined disulphide bridge introduction and proline residue substitution. Sci Rep-UK. 7:1-9.
38. Hakulinen N, Turunen O, Janis J, Leisola M, Rouvinen. 2003. Three-dimensional structures of thermophilic beta-1,4-xylanases from *Chaetomium thermophilum* and *Nonomuraea*

flexuosa. Comparison of twelve xylanases in relation to their thermal stability. Eur J Biochem. 270:1399-1412.

39. Asa B, Swc D, Ta E, Rta B. 2020. Biochemical characterization and molecular docking of cloned xylanase gene from *Bacillus subtilis* RTS expressed in *E. coli*. Int J Biol Macromol. 168:310-321.
40. Song Y, Lee YG, Choi IS, Lee KH, Bae HJ. 2013. Heterologous expression of endo-1,4-β-xylanase A from *Schizophyllum commune* in *Pichia pastoris* and functional characterization of the recombinant enzyme. Enzyme Microb Tech. 52:170-176.
41. Kalawong R, Wakayama M, Anuntalabhochai S, Wongsawad C, Sangwijit K. 2018. Comparison and characterization of purified cellulase and Xylanase from *bacillus amyloliquefaciens* CX1 and *bacillus subtilis* b4. Chiang Mai J Sci. 45:92-105.
42. Hamid A, Aftab MN. 2019. Cloning, Purification, and Characterization of Recombinant Thermostable β-Xylanase Tnap_0700 from *Thermotoga naphthophila*. Appl Biochem Biotech. 189:1-17.